中国物理学会
Chinese Physical Society

**RAPID COMMUNICATION**

# Emergence of correlations in twisted monolayer–trilayer graphene heterostructures

To cite this article: Zhang Zhou *et al* 2023 *Chinese Phys. B* **32** 097203

View the article online for updates and enhancements.

RAPID COMMUNICATION

# Emergence of correlations in twisted monolayer–trilayer graphene heterostructures

Zhang Zhou(周璋)[1,†], Kenji Watanabe[2], Takashi Taniguchi[2],
Xiao Lin(林晓)[1], Jinhai Mao(毛金海)[1,‡], and Hong-Jun Gao(高鸿钧)[3]

[1] *School of Physical Sciences and CAS Center for Excellence in Topological Quantum Computation,
University of Chinese Academy of Sciences, Beijing 100049, China*
[2] *Advanced Materials Laboratory, National Institute for Materials Science, Tsukuba, 305-0044, Japan*
[3] *Institute of Physics, Chinese Academy of Sciences, Beijing 100190, China*

Twisted bilayer graphene heterostructures have recently emerged as a well-established platform for studying strongly correlated phases, such as correlated insulating, superconducting, and topological states. Extending this notion to twisted multilayer graphene heterostructures has exhibited more diverse correlated phases, as some fundamental properties related to symmetry and band structures are correspondingly modified. Here, we report the observations of correlated states in twisted monolayer–trilayer (Bernal stacked) graphene heterostructures. Correlated phases at integer fillings of the moiré unit cell are revealed at a high displacement field and stabilized with a moderate magnetic field on the electron-doping side at a twist angle of $1.45°$, where the lift of degeneracy at the integer fillings is observed in the Landau fan diagram. Our results demonstrate the effectiveness of moiré engineering in an extended structure and provide insights into electric-field tunable correlated phases.

## 1. Introduction

Graphene-based moiré systems are emerging as a platform for creating novel quantum states, where the moiré Bloch bands form by tuning the weakly coupled Dirac electron with a periodic moiré potential.[1,2] The twisted bilayer graphene (tBG), as the simplest structure, demonstrates the effective formation of flat bands in both theory[3–5] and experiments.[6–10] Intuitively, the concept will also apply to twisted multilayer graphene. Specifically, twisted $(M + N)$-layer graphene is predicted to host two low-energy flat bands for each valley emerging from the interface between the $M$ and $N$ layers.[11–13] The extended structures successfully exhibit novel quantum phases, such as spin-polarized insulating states in twisted double-bilayer graphene (tDBG)[14–16] and quantum anomalous Hall effects in twisted monolayer–bilayer graphene (tMBG).[17]

Moving one step forward would involve stacking monolayer and trilayer graphene (TLG) together with just a single twist angle, which has been theoretically proposed to host correlated and topological states.[11,18] Notably, two stacking orders naturally exist in TLG, Bernal (ABA) stacking with mirror symmetry and rhombohedral (ABC) stacking with inversion symmetry,[19,20] where alternative degrees of freedom

are appreciated. When considering the structure of twisted monolayer–trilayer graphene (tMTG), the inversion symmetry is naturally absent, leading to the anticipation of electron–hole asymmetry and asymmetry with the direction of the displacement field at low-energy bands. Experimentally constructing the tMTG heterostructure would be rewarding to extend the family of graphene superlattices and to examine the evolution of correlation effects.

In this work, we investigate the electrical transport properties in tMTG (Bernal-stacking trilayer) dual-gated devices with twist angles of $1.45°$ and $1.51°$, and report clear observations of correlated phases. We find that the resistance peak at full fillings ($\nu = \pm 4$) and 'halo' regions are highly dependent on the charge density and displacement field. Correlated phases at commensurate fillings ($\nu = 1, 2$) of a moiré unit cell are revealed at a high displacement field ($D < -0.3$ V/nm) and stabilized with a specific magnetic field ($> 0.04\phi_0$, $\phi_0$ represents the quantum flux of the moiré unit cell) on the electron-doping side. The lifting of degeneracy is observed from the Landau fan diagram at the integer fillings. Our results have broadened the scope and enriched the family of twisted graphene moiré superlattices.

†Corresponding author. E-mail: zhouzhang1992@qq.com
‡Corresponding author. E-mail: jhmao@ucas.edu.cn

## 2. Twisted monolayer–trilayer graphene

The tMTG stacks in this work were fabricated by picking up the flakes sequentially following the van der Waals dry-transfer method.[21] See the fabrication details in the supporting information. The MLG and TLG were both obtained from one single flake to realize more precise control of the twist angle. Then, the assembled stacks were released onto a pre-patterned $SiO_2$/Si substrate and fabricated into multi-terminal Hall devices for transport measurements. A schematic of the whole device is shown in Fig. 1(a). An optical image of a typical device is shown in Figs. 1(b) and S1(a). The schematic moiré pattern is shown in Fig. 1(c), where the period is $\lambda = a/2\sin(\theta/2)$ with a relative twist angle $\theta$ and lattice constant of graphene $a = 2.46$ Å. In the ABA trilayer stacking, the top and bottom layers are overlapped from the top or bottom view; therefore, the schematic moiré pattern from the top view is the same as the tMBG. Gate tuning is independently applied through the metallic top gate and silicon bottom gate to tune the carrier density and displacement field continuously. The total charge doping density is $n = (C_{bg}V_{bg} + C_{tg}V_{tg})/e$ and the displacement field is $|D| = |C_{bg}V_{bg} - C_{tg}V_{tg}|/(2\varepsilon_0)$, where $\varepsilon_0$ is the vacuum permittivity, $V_{bg}$ and $V_{tg}$ are the effective gate voltages, and $C_{bg}$ and $C_{tg}$ are the capacitance per unit area of the bottom and top gate, respectively. The filling factor is $\nu = 4n/n_s$ where $n_s$ is the full-filling carrier density of the moiré unit cell.
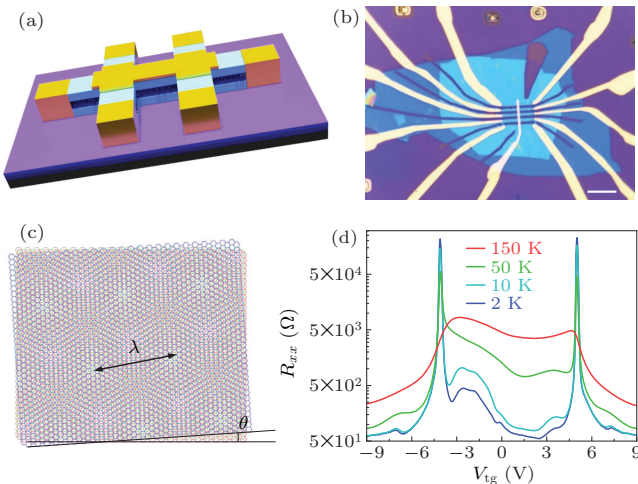


**Fig. 1.** Twisted monolayer–trilayer graphene. (a) A schematic of the tMTG device structure. The top gate is the gold electrode, and the bottom gate is Si/SiO₂. (b) An optical microscope image of the tMTG device. The scale bar is 10 μm. (c) An illustration of the moiré pattern of stacked tMBG graphene with the relative twist angle $\theta$. Here, $\lambda$ is the period of the moiré pattern. (d) The longitudinal resistance measured when scanning the top gate voltage ($V_{tg}$) with the bottom gate grounded. As the device is cooled down from 150 K to 2 K, two resistance peaks emerge at full filling of the moiré unit cell.

Transport measurements are conducted in a physical property measurement system (PPMS) in the four-terminal setup. As the device is cooled down, the common feature is the resistance peak emerging at the full filling state of the moiré unit cell, as shown in Fig. 1(d). When only scanning $V_{tg}$ with $V_{bg}$ set to 0, the onset temperature of resistance peaks as high as 150 K is observed, and the resistance peaks soon grow as the temperature decreases. This is a hallmark of twisted graphene moiré superlattices and indicates the single-particle energy gap between reconstructed flat bands and remote bands. The sheet resistance of the insulating state at 2 K is as high as $\sim 200$ kΩ at the insulating full filling state and drops sharply to as low as $\sim 0.1$ kΩ, with the difference greater than three orders of magnitude. The peaks of the three channels at full fillings coincide with each other in Fig. S2, indicating a uniform twist angle differing by less than $\pm 0.01°$ in the channel length of $\sim 5$ μm. The relative twisted angles are extracted from the carrier density at full fillings and further confirmed by the value of the quantum magnetic flux $\phi_0$ more precisely.
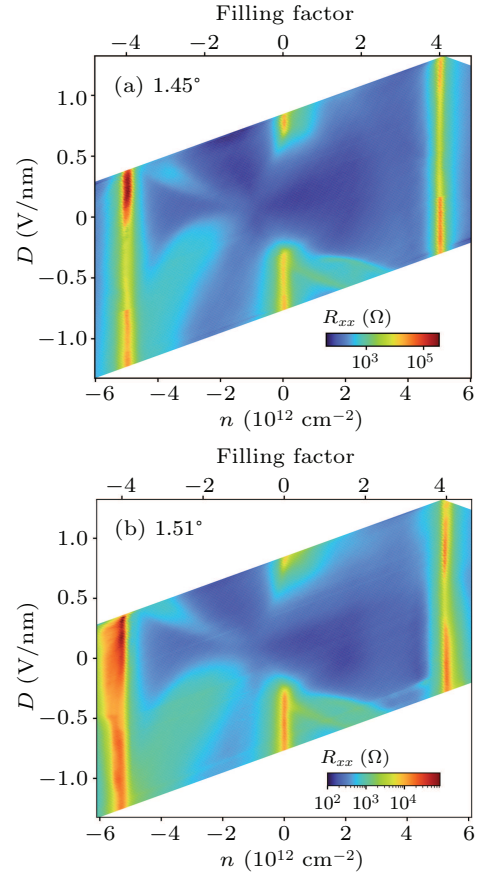


**Fig. 2.** The emergence of correlation in the tMTG devices. Mapping of the longitudinal resistance of the tMTG device on the carrier density $n$ (filling factor) and displacement field $D$ with twist angles of 1.45° (a) and 1.51° (b), measured at a temperature of 2.0 K and a magnetic field of 0 T.

The top and bottom gate voltages are then simultaneously scanned to obtain a detailed map of the longitudinal resistance, which is normalized to relations with $\nu$ and $D$, with the twisted angle of 1.45° in Fig. 2(a) and 1.51° in Fig. 2(b). The positive direction of $D$ is defined when the electric fields point

from TLG to MLG, for consistency when comparing different tMTG devices, considering the breaking of the mirror reflection symmetry. Resistance peaks emerge at full fillings at both the electron-doping and hole-doping sides. In the measured range of $D$ at the full fillings, the resistance is minimum at a relatively low $D$ and increases at both ends. On the hole side, 'cross-shaped' resistivity peaks emerge in the whole measured range of $D$, and the filling factor of the resistivity peak evolves with $D$ connecting the charge neutral point (CNP) and full fillings. On the electron side, high contrast 'halo' regions only emerge in the negative $D$ range, where the electron density is polarized and distributed mainly at the twisted interface.[22,23]

## 3. Tunable band structure

Next, we move on to revealing the correlated phase in detail on the device of $\theta = 1.45°$. As the temperature is cooled from 15 K to 2 K, the resistance peaks start to emerge near the integer fillings $\nu = 1$, 2, and 3 and near $\nu = -3$ in the $R_{xx}$ curve as a function of $\nu$ at a relatively large $D = -0.5$ V/nm, as shown in Fig. 3(a). These peaks could not be explained in the single-particle picture and indicate the onset of correlations. The relatively low resistance ($\sim 1$ k$\Omega$) and metallic behavior at $D < 0$ suggest that the correlation effects only cause partial gap opening or band overlaps, rather than the opening of bandgaps.
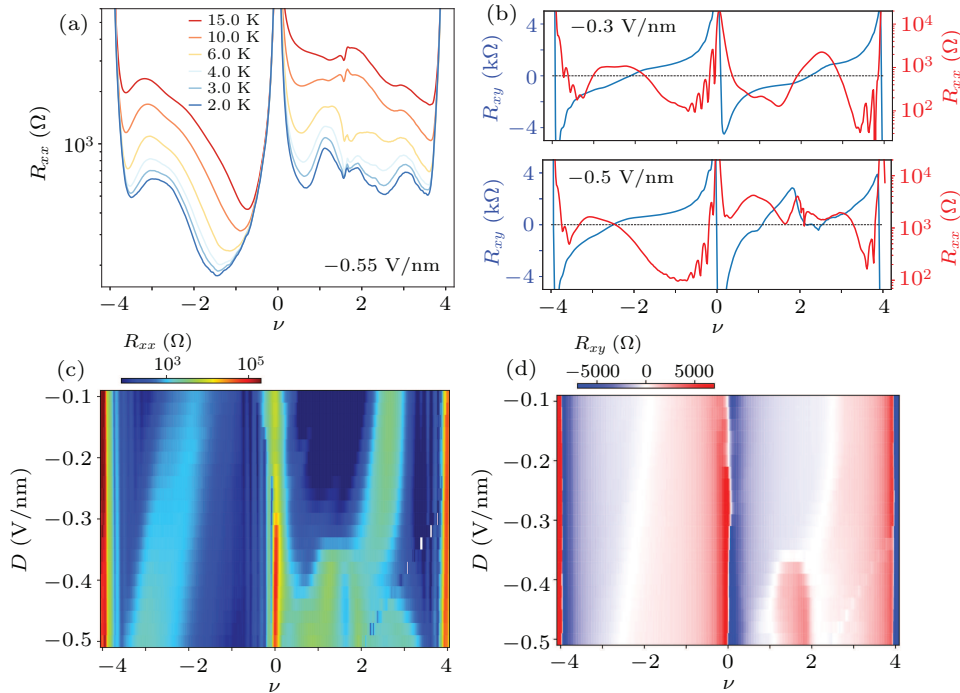


**Fig. 3.** Tunable band structure and transport properties of the tMTG device with $\theta = 1.45°$. (a) $R_{xx}$ as a function of the filling factor at $D = -0.55$ V/nm at a series of temperatures from 15 K to 2 K at $B = 0$. (b) $R_{xx}$ (red) and $R_{xy}$ (blue) as a function of the filling factor at $D = -0.3$ V/nm (top panel) and $-0.5$ V/nm (bottom panel) and $B = 2.0$ T. The horizontal dashed lines indicate $R_{xy} = 0$. (c), (d) Mapping of $R_{xx}$ (c) and $R_{xy}$ (d) on the filling factor and displacement field at an external magnetic field $B = 2.0$ T and temperature $T = 2.0$ K.

A magnetic field of 2 T ($< 0.05\phi_0$) is then applied to identify whether the band curvature is electron-like or hole-like, which is estimated based on the states where $R_{xy}$ changes sign, as shown in Fig. 3(b). These kinds of changes in the band curvature are typically related to van Hove singularities (vHSs). The vHSs appear on both the electron and hole sides and span the whole $D$ range from $-0.1$ V/nm to $-0.5$ V/nm, as depicted in Fig. 3(d). For ease of comparison, Fig. 3(b) depicts two panels exhibiting the $R_{xx}$ (red) and $R_{xy}$ (blue) as a function of the filling factor at $D = -0.3$ V/nm and $-0.5$ V/nm, respectively. As demonstrated in Fig. 3(b), $R_{xx}$ peaks emerge at the positions of vHSs, and the sign of $R_{xy}$ changes correspondingly. Moreover, the positions of vHSs evolve with $D$. The white stripes (vHSs, $R_{xy} = 0$) on both the electron and hole sides of

Fig. 3(d) show the same trend as the position of the peaks in Fig. 3(c). The change in $R_{xy}$'s sign is commonly related to saddle points in the momentum space, which is comparable to the tBG and tMBG devices.[24,25]

Despite applying a relatively weak magnetic field, the correlated phases are considerably strengthened, as depicted by the comparison between Figs. 3(c) and S3(a). As observed on the electron-doping side, the central position of the high-contrast stripe evolves from $\nu = 3$ to 2 when $D$ increases from $-0.1$ V/nm to $-0.35$ V/nm. Above $D = -0.35$ V/nm, the single peak sharply splits into two peaks, which appear around commensurate fillings of $\nu = 1$ and 2 and remain unchanged with $D$. The corresponding changes are also observed in the $R_{xy}$ mapping, as shown in Fig. 3(d). Notably, the magnetore-

sistance (Shubnikov–de Haas, SdH) oscillations are observed around resistance peaks close to the CNP and full fillings in both panels of Fig. 3(b). Furthermore, additional oscillations near $\nu = 2$ are found at $D = -0.5$ V/nm in the bottom panel, which suggests new band edge formation due to enhanced electron correlations at the half-filling.

It is therefore intriguing to systematically reveal the detailed magneto oscillation evolution with the magnetic field, which could provide insights into the Fermi surface and degeneracy associated with electronic degrees of freedom. A perpendicular magnetic field ($B$) will have impacts on graphene moiré superlattices in two different ways. First, the magnetic field would induce splitting between the flat bands with opposite Chern numbers due to the orbital Zeeman effect, which assists to isolate and stabilize the flat bands. Second, the magnetic field tends to recombine the flat bands into a sequence of fractal Landau levels (LLs), also known as Hofstadter's butterfly spectra,[26] in which the recurring fractal bands are dependent on the number of magnetic fluxes in each moiré primitive cell. The Landau fan diagram for the tMTG device of 1.45° at $D = -0.5$ V/nm and $T = 2.0$ K is presented in Fig. 4(a). In the hole-doping region, the Landau fan exhibits a complex Hofstadter's butterfly pattern. The pattern reveals the crossing of Landau levels from the CNP and the full filling of holes, as a result of commensurate flux threading into the unit cell. Fractional fillings of $\frac{1}{9}\phi_0$, $\frac{1}{8}\phi_0$, $\frac{1}{7}\phi_0$ and $\frac{1}{6}\phi_0$ could be identified and are emphasized with horizontal dashed lines.
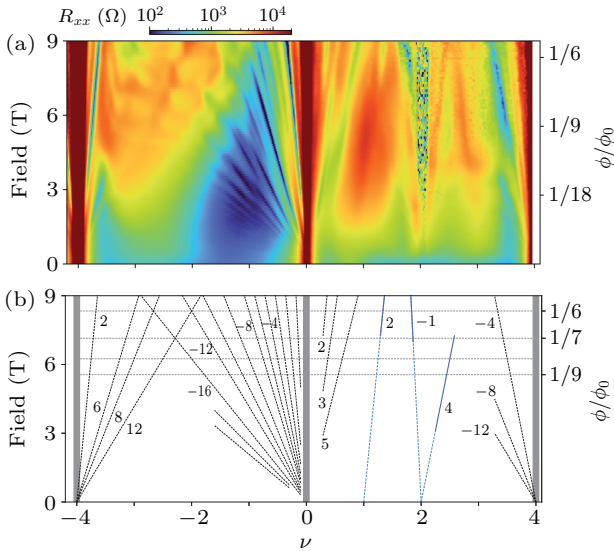


**Fig. 4.** Quantum oscillations in the tMTG device with $\theta = 1.45°$ at $D = -0.5$ V/nm and $T = 2.0$ K. (a) The Landau fan diagram on the tMTG device. Numbers at the right $y$-axis indicate $\phi/\phi_0$ fractions, where $\phi_0 = h/e$, $h$ is the Planck constant, $e$ is the electron charge, and $\phi = BS$ is magnetic flux through a moiré unit cell. The Landau-level structure extracted from the oscillations is plotted in (b). The tilted dashed lines correspond to the Landau levels, with sequences labelled. The blue lines originate from the filling factors $\upsilon = 1$ and 2. The black lines originate from the charge neutrality point (CNP), and full fillings of the moiré unit cell at both the electron and hole sides. The horizontal dashed lines indicate fractal values 1/6, 1/7, 1/8 and 1/9 of $\phi/\phi_0$.

We observe linearly dispersing features on the electron side emanating from integer fillings. The linearly dispersing features can be characterized by fitting the Diophantine equation (Fig. 4(b)), $\nu = C\phi/\phi_0 + \nu_0$, where $\phi$ is the magnetic flux per moiré unit cell, $\phi_0 = h/e$ is the flux quantum, $h$ is Planck's constant, $e$ is the elementary charge of an electron, and $\nu_0$ is the band filling index or the number of carriers per unit cell at $B = 0$ T. Trajectories emanating from the CNP, $\nu_0 = 0$, despite being unaffected by the moiré potential, still form a bilateral Landau fan. Specifically, the LLs of $C = -1, -2, -3, -4, -5, -6, -8, -10, -12, -16, \ldots$ on the hole-doping side mainly contribute to the fan. Meanwhile, on the electron-doping side, only LLs of $C = 2, 3, 5$ could be distinguished, displaying a fully lifted degeneracy. At the full filling of holes ($\nu_0 = -4$), the LLs of $C = 2, 6, 8$, and 12 are observed at symmetry broken to two-fold degeneracy, while at the full filling of electrons ($\nu_0 = 4$), the LLs of $C = -4, -8$, and $-12$ are observed, indicating four-fold degeneracy.

Notably, the correlated phase is enhanced with the increase in the magnetic field. The feature ($C = 2$) fanning from $\nu_0 = 1$ starts emerging from the field of $\frac{1}{7}\phi_0$ at the electron branch. For the two linear features fanning from $\nu_0 = 2$, the $C = -1$ feature starts emerging at around $\frac{1}{7}\phi_0$ at the hole side, and the $C = 4$ feature emerges at a relatively low field. No additional features have been found to decipher the remaining degeneracy. This is consistent with previous studies of tBG and tMBG, in which STM/STS measurements have indicated that a Dirac-like dispersion is revived at each quarter band filling due to a cascade of spontaneously broken symmetries.[28,29]

In summary, we report the observation of a correlated phase in a tMTG structure with twist angles of 1.45° and 1.51°. The correlated phase of the tMTG structure exhibits similarities to tMBG regarding the broken mirror symmetry and electron-hole asymmetry. These correlated phases are revealed only under a relatively large displacement field and are stabilized under a moderate magnetic field. Our findings have expanded the parameter space of the twisted graphene family, and may stimulate further research on twisted multilayer graphene.

## Acknowledgements

## References

[1] Bistritzer R and MacDonald A H 2011 *Proc. Natl. Acad. Sci.* **108** 12233

[2] Andrei E Y, Efetov D K, Jarillo-Herrero P, MacDonald A H, Mak K F, Senthil T, Tutuc E, Yazdani A and Young A F 2021 *Nat. Rev. Mater.* **6** 201

[3] Song Z, Wang Z, Shi W, Li G, Fang C and Bernevig B A 2019 *Phys. Rev. Lett.* **123** 036401

[4] Tarnopolsky G, Kruchkov A J and Vishwanath A 2019 *Phys. Rev. Lett.* **122** 106405

[5] Liu J and Dai X 2021 *Phys. Rev. B* **103** 035427

[6] Cao Y, Fatemi V, Demir A, Fang S, Tomarken S L, Luo J Y, Sanchez-Yamagishi J D, Watanabe K, Taniguchi T, Kaxiras E, Ashoori R C and Jarillo-Herrero P 2018 *Nature* **556** 80

[7] Cao Y, Fatemi V, Fang S, Watanabe K, Taniguchi T, Kaxiras E and Jarillo-Herrero P 2018 *Nature* **556** 43

[8] Lu X, Stepanov P, Yang W, Xie M, Aamir M A, Das I, Urgell C, Watanabe K, Taniguchi T, Zhang G, Bachtold A, MacDonald A H and Efetov D K 2019 *Nature* **574** 653

[9] Serlin M, Tschirhart C L, Polshyn H, Zhang Y, Zhu J, Watanabe K, Taniguchi T, Balents L and Young A F 2020 *Science* **367** 900

[10] Waters D, Thompson E, Arreguin-Martinez E, Fujimoto M, Ren Y, Watanabe K, Taniguchi T, Cao T, Xiao D and Yankowitz M 2022 arXiv: 2211.15606 [cond-mat]

[11] Liu J, Ma Z, Gao J and Dai X 2019 *Phys. Rev. X* **9** 031021

[12] Wang J and Liu Z 2022 *Phys. Rev. Lett.* **128** 176403

[13] Ledwith P J, Vishwanath A and Khalaf E 2022 *Phys. Rev. Lett.* **128** 176404

[14] Cao Y, Rodan-Legrain D, Rubies-Bigorda O, Park J M, Watanabe K, Taniguchi T and Jarillo-Herrero P 2020 *Nature* **583** 215

[15] Liu X, Hao Z, Khalaf E, Lee J Y, Ronen Y, Yoo H, Haei Najafabadi D, Watanabe K, Taniguchi T, Vishwanath A and Kim P 2020 *Nature* **583** 221

[16] Shen C, Chu Y, Wu Q, Li N, Wang S, Zhao Y, Tang J, Liu J, Tian J, Watanabe K, Taniguchi T, Yang R, Meng Z Y, Shi D, Yazev O V and Zhang G 2020 *Nat. Phys.* **16** 520

[17] Polshyn H, Zhu J, Kumar M A, Zhang Y, Yang F, Tschirhart C L, Serlin M, Watanabe K, Taniguchi T, MacDonald A H and Young A F 2020 *Nature* **588** 66

[18] Goodwin Z A H, Klebl L, Vitale V, Liang X, Gogtay V, van Gorp X, Kennes D M, Mostofi A A and Lischner J 2021 *Phys. Rev. Mater.* **5** 084008

[19] Bao W, Jing L, Velasco J, Lee Y, Liu G, Tran D, Standley B, Aykol M, Cronin S B, Smirnov D, Koshino M, McCann E, Bockrath M and Lau C N 2011 *Nat. Phys.* **7** 948

[20] Lui C H, Li Z, Mak K F, Cappelluti E and Heinz T F 2011 *Nat. Phys.* **7** 944

[21] Wang L, Meric I, Huang P Y, Gao Q, Gao Y, Tran H, Taniguchi T, Watanabe K, Campos L M, Muller D A, Guo J, Kim P, Hone J, Shepard K L and Dean C R 2013 *Science* **342** 614

[22] Chen S, He M, Zhang Y-H, Hsieh V, Fei Z, Watanabe K, Taniguchi T, Cobden D H, Xu X, Dean C R and Yankowitz M 2021 *Nat. Phys.* **17** 374

[23] Li S, Wang Z, Xue Y, Wang Y, Zhang S, Liu J, Zhu Z, Watanabe K, Taniguchi T, Gao H, Jiang Y and Mao J 2022 *Nat. Commun.* **13** 4225

[24] Wu S, Zhang Z, Watanabe K, Taniguchi T and Andrei E Y 2021 *Nat. Mater.* **20** 488

[25] Xu S, Al Ezzi M M, Balakrishnan N, Garcia-Ruiz A, Tsim B, Mullan C, Barrier J, Xin N, Piot B A, Taniguchi T, Watanabe K, Carvalho A, Mishchenko A, Geim A K, Fal'ko V I, Adam S, Neto A H C, Novoselov K S and Shi Y 2021 *Nat. Phys.* **17** 619

[26] Hofstadter D R 1976 *Phys. Rev. B* **14** 2239

[27] Streda P 1982 *J. Phys. C Solid State Phys.* **15** L1299

[28] Wong D, Nuckolls K P, Oh M, Lian B, Xie Y, Jeon S, Watanabe K, Taniguchi T, Bernevig B A and Yazdani A 2020 *Nature* **582** 198

[29] He M, Zhang Y H, Li Y, Fei Z, Watanabe K, Taniguchi T, Xu X and Yankowitz M 2021 *Nat. Commun.* **12** 4727

[30] Huang Y, Sutter E, Shi N N, Zheng J, Yang T, Englund D, Gao H J and Sutter P 2015 *ACS Nano* **9** 10612